International Archive of Applied Sciences and Technology, Vol 1 [2] December 2010: 20 - 28

ISSN 0976- 4828
http:// www.soeagra.com

RESEARCH ARTICLE

Electron Transport Characteristics of 6h-Sic and 4h-Sic for High Temperature Device Modeling

H. Arabshahi and M. Rezaee Rokn-Abadi
Physics Department, Ferdowsi University of Mashhad, Mashhad, Iran
E-mail: .arabshahi@um.ac.ir

ABSTRACT

The Monte Carlo method is used to simulate electron transport in bulk wurtzite phases of 6H-SiC and 4H-SiC using a three valley analytical band structure. Spherical, non-parabolic conduction band valleys at the Γ, K and U symmetry points of the Brillouin zone are fitted to the first-principles band structure. The electron drift velocity is calculated as a function of temperature and ionized donor concentration in the ranges of 300-600 K and 10^{16}-10^{20} cm^{-3}, respectively. Due to the freezout of deep donor levels the role of ionized impurity scattering in 6H-SiC is suppressed and the role of phonon scattering is enhanced, compared to 4H-SiC. For two materials, it is found that electron velocity overshoot only occurs when the electric field is increased to a value above a certain field unique to each material. This critical field is strongly dependent on the material parameters.

***KEY WORDS**: Monte Carlo; non-parabolic; velocity overshoot; ionized donor; Brillouin zone.*

INTRODUCTION

SiC poly-types are being proposed for electronic and photonic devices operating under high-temperature and high-power conditions, mainly due to its highly suited thermal and transport properties [1-5]. Although material growth and characterization issues have been extensively addressed in the literature, there have been few experimental efforts to investigate electronic characterization of SiC poly-types. This is due to the difficulty in sample preparation that prevailed for several years. Strong and recent research efforts resulted from the technological advances in the SiC poly-types growth processes [6-10] and propelled the characterization of their band structure, electrical, and optical properties [11-13]. Their theoretical electron transport properties were studied in the past years, including the investigation of the steady–state behavior [14-16] high–frequency transport properties [17] and more recently the ultrafast transient response [18]. Strong field effects on SiC polytypes were investigated either through Monte Carlo simulation, quantum transport based and Boltzmann-like equations [19].

The purpose of this work is to present a study on the influence of the lattice temperature and ionized donor concentration in the hot electron mobility in 6H-SiC and 4H-SiC subjected to a high applied electric field along the hexagonal c-axis direction in the wurtzite material. The focus on these SiC poly-types is due to their potential applications associated with their high saturation velocities, particularly in the domain of high temperature and high-speed/high-field nanostructures.

The transport properties are calculated through the numerical solution of the Boltzmann transport equation by Monte Carlo technique. This paper is organized as follows. Details of the Monte Carlo model and the electron scattering mechanisms calculations are presented in section 2 and the results of Monte Carlo simulations carried out on 6H-SiC and 4H-SiC structures are interpreted in section 3.

METHOD OF CALCULATIONS

The principle of the Monte Carlo method as applied to the determination of distribution functions is to simulate the motion of one electron in momentum space. This motion consists alternately of a drift with constant velocity in the electric field followed by a scattering by phonons. The time which the electron drifts in the electric field, the type of scattering process and the final state are random quantities with probability distributions which can be expresses in terms of the transition rates due to the various processes and the strength of the electric field. These probability distributions, however, can be quite complex, particularly that for the drift time, whereas it is only straightforward to generate by computer random numbers with equal probability over some finite range. As a result techniques

are required to convert this equal probability distribution into the complex distributions required here. Suppose that the transition rate between two wave vector states *k* and *k'* is *Sq*(*k*, *k'*). Here the subscript q denotes the scattering process and can take the values q= 1, 2,...*N*, if there are *N* possible processes. The probability per unit time that the electron will drift for a time *t* in an electric field *E* and then be scattered is given by

$$p(t) = \lambda[k(t)] \exp\left\{-\int_0^t \lambda[k(t')]dt'\right\} \qquad (1)$$

where

$k(t) = k_0 + eEt/\hbar$, $\lambda(k) = \sum_{q=1}^{N} \lambda_q(k)$ and $\lambda_q(k) = \int dk' S_q(k,k')$ is the total transition rate from the state *k* due to the *q*-th process. Also k_0 is the wave vector at *t*=0 at the beginning of the flight, i.e. the final state after the previous scattering event. The procedure adopted from by Kurosawa [20] to generate random times from the probability distribution was to use random numbers *r* generated with equal probability between 0 and 1. Then using *P(r)dr=P(t)dt* we obtain

$$r = \int_0^t P(t')dt' \quad \text{or} \quad r = 1 - \exp\left\{-\int_0^t \lambda[k(t')]dt'\right\} \qquad (2)$$

For some scattering processes the integral in 2 can be evaluated analytically and *t* determined from a random number *r* analytically or numerically. However, the complicated form of *Sq*(*k*, *k'*) for some of the scattering processes considered here means that the integral can not be evaluated analytically and *t* can then be determined from *r* only by solving the integral equation or by interpolation in a numerical table of λ as a function of *t* and the initial components of *k*. Instead of these possibilities an alternative technique has been used to generate times from the distribution 1. Suppose in addition to the real scattering processes present in the semiconductor we include a fictitious processes for which

$$S_0(k,k') = \lambda_0(k)\delta(k-k') \qquad (3)$$

Since the delta function does not allow the electron wave vector to change in the scattering event, this self-scattering process is of no physical significance and then the function $\lambda_0(k)$ is completely arbitrary. Including this additional process in equation 1 leads to

$$P(t) = \lambda_0[k(t)] + \lambda[k(t)] \times \exp\left\{-\int_0^t (\lambda_0[k(t')] + \lambda[k(t')]dt'\right\} \qquad (4)$$

and we can now choose $\lambda_0(k)$ in such a way that the exponential factor becomes simple. The particular choice which has been made for $\lambda_0(k)$ in the present work is

$$\lambda_0(k) = \Gamma - \lambda(k) \qquad (5)$$

where Γ is constant. This choice for $\lambda_0(k)$, while not necessarily the optimum expression, has the advantage that 4 becomes simply

$$P(t) = \Gamma e^{-\Gamma t} \qquad (6)$$

and so has the effect of simulating the motion of an electron that has an energy-independent relaxation time of 1/Γ. The constant Γ is taken to be at least as large as the largest value of λ(*k*) of interest in order to avoid negative values of $\lambda_0(k)$. The effect of including the self-scattering process is to subdivide the real flight of the electron into shorter flights of duration governed by the probability distribution 5. It is possible to see this in an entirely mathematical way by writing the original probability distribution 1 in the form

$$P(t) = \lambda(t)e^{-\Gamma t} \exp\left\{\int_0^t [\Gamma - \lambda(t')]dt'\right\} \qquad (7)$$

where for simplicity we have written λ[*k*(*t*)] as λ(*t*). Having determined the time of free flight, it is necessary to determine the scattering process responsible for terminating the flight. Since the probability of the electron being scattered by process *q* is proportional to $\lambda_q(k)$ and since $\sum_{q=0}^{N} \lambda_q = \Gamma$, it is only necessary to generate a random number *S* between 0 and Γ and test the inequality

$$S \le \sum_{q=0}^{m} \lambda_q(k) \qquad (8)$$

for all *m*. When this inequality is satisfied, the scattering process *m* is selected. It is at this stage that the only disadvantage of using the simple distribution 3 is made apparent, because there is now a finite probability of self-scattering being selected. Since this process does not change the electron wave vector, it does not contribute to the determination of the distribution function. It is clearly an advantage to make Γ as small as possible in order to make the number of self-scattering events a minimum. Despite this disadvantage, it is still more efficient to include self-scattering than to work directly with the distribution 1, particularly since the final state after the self-scattering is known.

For all real processes, further random numbers are required to determine the final state after the scattering. It is convenient to regard phonon absorption and emission as separate processes in 7. Then the energy of the final state is also determined by this inequality for all the processes considered here, since the energy change is either independent of the change in momentum, as in polar and inter-valley scattering, or zero as in acoustic scattering. We note that this would not be the case if the acoustic phonon energy were kept finite, when a more complicated procedure would be required. However, in the present case it then only remains to determine the components of *k* corresponding to this energy after the scattering event.

In order to calculate the electron transport properties in semiconductors and devices, we must identify the important electron scattering mechanisms. In a semiconductor, there are a number of physical processes which can cause an electron in a certain state to be scattered. The relative importance of each scattering process in a given material depends on the electric field strength and the material properties. When an electron is scattered, the wave vector of the electron is changed from an initial wave vector *k* to some final wave vector *k′*. The time required for a scattering process to change the wave vector from *k* to *k′* is called the collision duration τ_c. Here we assume collisions occur with τ_c=0. The inclusion of a scattering in transport calculations normally requires the formulation of the total scattering rate and angular dependence of the scattering between state *k* and state *k′*. The transition rate *S*(*k*, *k′*) from state *k* to state *k′* is normally calculated by using Fermi's golden rule

$$S(k,k') = \frac{2\pi}{\hbar}\int \left|\langle k'|\, H \,|\, k\rangle\right|^2 G(k,k') \times \delta[E(k') - E(k) \pm \Delta E]\, d^3k' \qquad (9)$$

where $\int \left|\langle k'|\, H \,|\, k\rangle\right|^2$ is the matrix element between plane wave functions of the perturbing Hamiltonian describing the scattering agency, ΔE is the energy gain (+) or loss (-) during the transition and the integration is over all final states restricted by the energy conserving delta function. *G*(*k*,*k′*) is the overlap integral between the periodic parts of the Bloch periodic functions of the initial and final states. The overlap integral is exactly equal to unity for pure *s*-state wave functions (parabolic conduction bands). When the non-periodicity of the bands is taken into account, the overlap integral is always less than one and is usually expressed as a function of the non-periodicity coefficients. Once the overlap integral between the periodic parts of the Bloch functions at *k* and *k′* are known the total scattering rate *R*(*k*) can be calculated by integrating *S*(*k*, *k′*) in equation 9 over all allowed final states [21-22]

$$R(k) = \frac{V}{8\pi^3}\iiint S(k,k')k'^2 \sin\theta d\theta d\varphi dk' \qquad (10)$$

where *V* is the volume of the crystal.

The scattering mechanisms can be classified into two main types, those due to lattice vibrations and called lattice (or phonon) scattering and defect scattering due to ionized impurities and alloy disorder. In the following sections the behavior of the electron scattering rates as a function of energy will be shown for various scattering processes.

A. Deformation potential scattering

The acoustic modes modulate the inter-atomic spacing. Consequently, the position of the conduction and valence band edges and the energy band gap will vary with position because of the sensitivity of the band structure to the lattice spacing. The energy change of a band edge due to this mechanism is defined by a deformation potential and the resultant scattering of carriers is called deformation potential scattering. The energy range involved in the case of scattering by acoustic phonons is from

zero to $2\hbar vk$, where v is the velocity of sound, since momentum conservation restricts the change of phonon wave-vector to between zero and 2k, where k is the electron wave-vector. Typically, the average value of k is of the order of 10^7 cm^{-1} and the velocity of sound in the medium is of the order of 10^5 cms^{-1}. Hence, $2\hbar vk$ ~ 1 meV , which is small compared to the thermal energy at room temperature. Therefore, the deformation potential scattering by acoustic modes can be considered as an elastic process except at very low temperature. The deformation potential scattering rate with either phonon emission or absorption for an electron of energy E in a non-parabolic band is given by Fermi's golden rule as [8-9]

$$R_{de}(k)=\frac{\sqrt{2}D_{ac}^2(m_t^{*2}m_l^*)^{1/2}K_BT}{\pi\rho v^2\hbar^4}\frac{\sqrt{E(1+\alpha E)}}{(1+2\alpha E)}\left[(1+\alpha E)^2+1/3(\alpha E)^2\right] \qquad (11)$$

where D_{ac} is the acoustic deformation potential, ρ is the material density and α is the non-parabolicity coefficient. The formula clearly shows that the acoustic scattering increases with temperature.

B. Piezoelectric scattering

The second type of electron scattering by acoustic modes occurs when the displacements of the atoms create an electric field through the piezoelectric effect. This can occur in the compound semiconductors such as the III-V and II-VI materials including SiC, which in fact has a relatively large piezoelectric constant. The piezoelectric scattering rate for an electron of energy *E* in an isotropic, parabolic band has been discussed by Ridley [10] who included the modification of the Coulomb potential due to free carrier screening. The screened Coulomb potential is written as

$$V(r)=\frac{e^2}{4\pi\varepsilon_0\varepsilon_s}\frac{\exp(-q_0r)}{r} \qquad (12)$$

where ε_s is the relative dielectric constant of the material and q_0 is the inverse screening length, which under non-degenerate conditions is given by

$$q_0^2=\frac{ne^2}{\varepsilon_0\varepsilon_s K_BT} \qquad (13)$$

where n is the electron density. The expression for the scattering rate of an electron in a non-parabolic band structure retaining only the important terms can be written as [8-9]

$$R_{pz}(k)=\frac{\sqrt{m^*}e^2K_{av}^2K_BT}{4\sqrt{2}\pi\hbar^2\varepsilon_0\varepsilon_s}\gamma^{-1/2}(E)(1+2\alpha E)^2\times \left[\ln(1+\frac{8m^*\gamma(E)}{\hbar^2q_0^2}-\frac{1}{1+\hbar^2q_0^2/8m^*\gamma(E)}+\left(\frac{\sqrt{2}\alpha E}{1+2\alpha E}\right)^2\right] \qquad (14)$$

where K_{av} is the dimensionless so called average electromechanical coupling constant.

C. Polar Optical Phonon Scattering

The dipolar electric field arising from the opposite displacement of the negatively and positively charged atoms provides a coupling between the electrons and the lattice which results in electron scattering. This type of scattering is called polar optical phonon scattering and at room temperature is generally the most important scattering mechanism for electrons in III-V semiconductors, and this is also the case in SiC despite the fact that the optical phonon energy is particularly high at ~ 93 meV which suppresses the phonon population and also electrons must reach that energy before phonon emission is possible. The scattering rate due to this process for an electron of energy E in an isotropic, non-parabolic band is [8-9]

$$R_{po}(k)=\frac{\sqrt{2m^*}e^2\omega_{op}}{8\pi\varepsilon_0\hbar}\left(\frac{1}{\varepsilon_\infty}-\frac{1}{\varepsilon_s}\right)\frac{1+2\alpha E'}{\gamma^{1/2}(E)}\times F_0(E,E')\{N_{op},N_{op}+1\} \qquad (15)$$

where

$$F_0(E,E') = C^{-1}\left\{A\ln\left|\frac{\gamma(E)^{1/2}+\gamma(E')^{1/2}}{\gamma(E)^{1/2}-\gamma(E')^{1/2}}\right| + B\right\}$$

$$A = \left[2(1+\alpha E)(1+\alpha E') + \alpha(\gamma+\gamma')\right]^2$$

$$B = -2\alpha\gamma^{1/2}\gamma'^{1/2}\left[4(1+\alpha E)(1+\alpha E') + \alpha(\gamma+\gamma')\right]$$

$$C = 4(1+\alpha E)(1+\alpha E')(1+2\alpha E)(1+2\alpha E')$$

where N_{op} is the phonon occupation number and the upper and lower cases refer to absorption and emission, respectively. For small electric fields, the phonon population will be very close to equilibrium so that the average number of phonons is given by the Bose-Einstein distribution

$$N_{op} = \frac{1}{\exp(\frac{\hbar\omega_{op}}{K_B T}) - 1} \qquad (16)$$

where $\hbar\omega_{op}$ is the polar optical phonon energy.

D. Non-polar Optical Phonon Scattering

Non-polar optical phonon scattering is similar to deformation potential scattering,in that the deformation of the lattice produces a perturbing potential but in this case the deformation is carried by optical vibrations. The non-polar optical phonon scattering rate in non-parabolic bands is given by[8,9].

$$R_{npo}(k) = \frac{D_{od}^2 (m_t^{*2} m_l^*)^{1/2}}{\sqrt{2}\pi\hbar^3\rho\omega_{op}}(1+2\alpha E)\gamma^{1/2}(E)\left[N_{op}, N_{op}+1\right] \qquad (17)$$

where D_{od} is the optical deformation potential and $E = E' \pm \hbar\omega_{op}$ is the final state energy phonon absorption (upper case) and emission (lower case).

E. Impurity Scattering

This scattering process arises as a result of the presence of impurities in a semiconductor. The substitution of an impurity atom on a lattice site will perturb the periodic crystal potential and result in scattering of an electron. Since the mass of the impurity greatly exceeds that of an electron and the impurity is bonded to neighboring atoms, this scattering is very close to being elastic. Ionized impurity scattering is dominant at low temperatures because, as the thermal velocity of the electrons decreases, the effect of long-range Coulombic interactions on their motion is increased. The electron scattering by ionized impurity centers has been discussed by Brooks-Herring [22-24] who included the modification of the Coulomb potential due to free carrier screening. The scattering rate for an isotropic, non-parabolic band structure is given by [8-9]

$$R_{im}(k) = \frac{8\pi n_i e^4}{k_s^2\hbar q_0}(m_t^{*2} m_l^*)^{1/2}\gamma^{1/2}(E)\frac{1+2\alpha E}{1+4\sqrt{2}\gamma(E)(m_t^{*2} m_l^*)^{1/6}/\hbar q_0} \qquad (18)$$

where n_i is the impurity concentration, q_0 is the screening length and k_s is the dielectric constant of the material.

RESULTS AND DISCUSSION

Electron drift velocity as a function of electric field and electron donor concentration are important in determining the performance of high-speed and microwave semiconductor devices. Here we show the results of temperature and doping dependencies of the steady-state
velocity-field characteristics and valley occupancy in the bulk 6H-SiC and 4H-SiC crystal structures. Figure 1 shows the simulated velocity-field characteristic of these two structures at 300 K, with a background doping concentration of 10^{16} cm^{-3}, and with the electric field applied along the hexagonal *c*-axis. The peak drift velocity for 4H-SiC and 6H-SiC are ~1.25×10^5 and 10^5 ms^{-1}, respectively. At higher electric fields, inter-valley optical phonon emission dominates, causing the drift velocity to

saturate at around 0.75×10^5 ms^{-1} for both phases. The threshold field for the onset of significant scattering into satellite conduction band valleys is a function of the inter-valley separation and the density of electronic states in the satellite valleys.
The average carrier kinetic energy as a function of electric field is shown in figure 2, for 6H-SiC (bold circle) and 4H-SiC (open circle). The curves have the typical form of other III-V compounds, which is a consequence of inter-valley transfer. At high fields, the curve for 6H-SiC suggests that the average electron energy is higher than for 4H-SiC. This difference can be understood by considering the valley occupancy as a function of field.

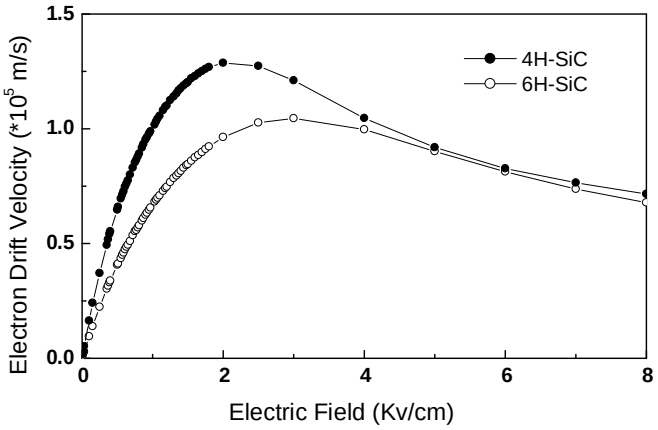

Figure 1: Calculated steady-state electron drift velocity in bulk 6H-SiC and 4H-SiC using the non-parabolic band models room temperature.

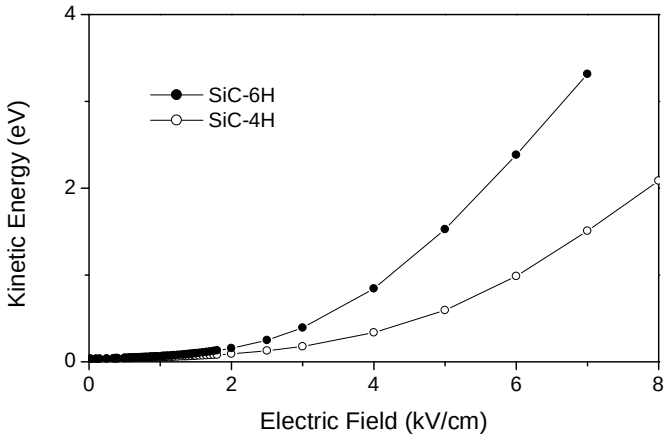

Figure 2: Average electron kinetic energy as a function of applied electric field in bulk 6H-SiC and 4H-SiC using the non-parabolic band models room temperature.

The importance of electron inter-valley transfer at high electric fields can be clearly seen in figure 3. In these figures the fractional valley occupancies for both phases of SiC are plotted. It is obvious that the inclusion of satellite valleys in the simulations is important. Significant electron transfer to the upper valleys only begins to occur when the field strength is very close to the threshold value. At the threshold field the electron valley occupancies for Γ, U are K are about %95, %4 and %1, respectively. As it can be seen, inter-valley transfer is substantially larger in the 4H-SiC than 6H-SiC, due to the combined effect of a lower Γ-valley effective mass, lower satellite valley separation and reduced phonon scattering rate within the Γ-valley, but significant inter-valley phonon scattering at a threshold field of 2 kV/cm.

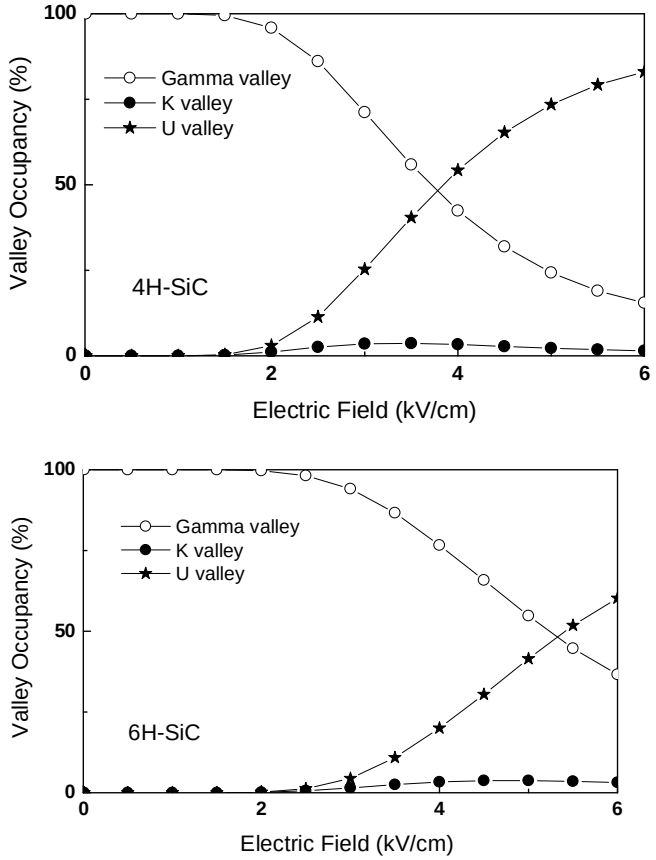

Figure 3: Fractional occupation of the central Γ and satellite valleys of 6H-SiC and 4H-SiC as a function of applied electric field using the non-parabolic band models room temperature.

Figure 4 shows the calculated electron drift velocity as a function of electric field strength for temperatures of 300, 450 and 600 K. The decrease in drift mobility with temperature at low fields is due to increased intra-valley polar optical phonon scattering whereas the decrease in velocity at higher fields is due to increased intra and inter-valley scattering. It can be seen from the figure that the peak velocity also decreases and moves to higher electric field as the temperature is increased. This is due to the general increase of total scattering rate with temperature, which suppresses the electron energy and reduces the population of the satellite valleys. This latter effect is apparent from the fact that the electron population in the Γ-valley increases with temperature.

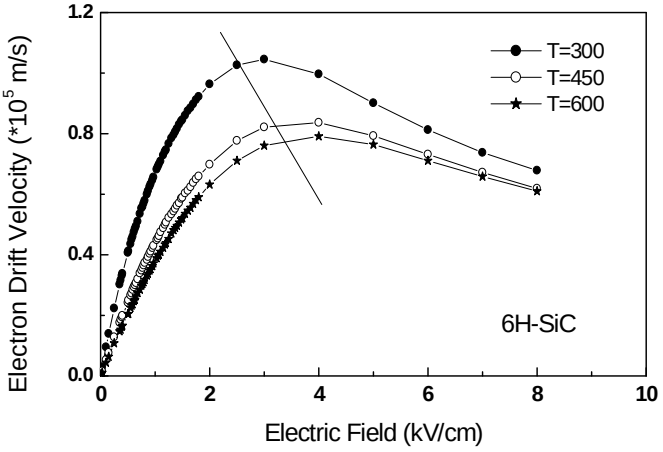

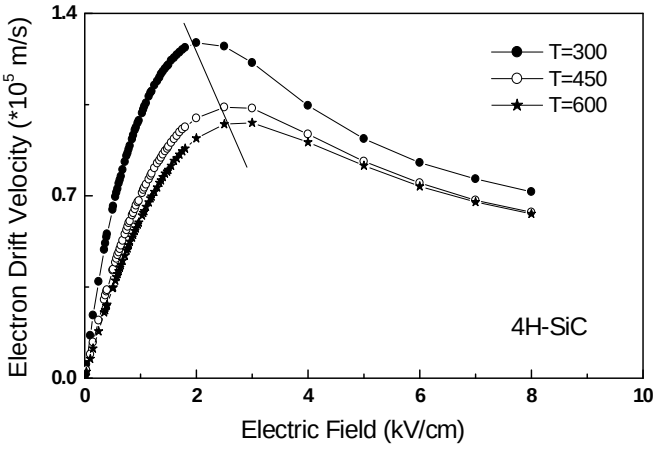

Figure 4: Calculated electron steady-state drift velocity in bulk 6H-SiC and 4H-SiC as a function of applied electric field at various lattice temperatures and assuming a donor concentration of 10^{16} cm^{-3}. The peak drift velocity decreases by about %5 while the threshold field increases by same percent as the lattice temperature increases from 300 to 600 K.

Figure 5 shows how the velocity-field characteristic of 6H-SiC and 4H-SiC change with impurity concentration at 300 K. It is clear that with increasing donor concentration, there are small changes in the average peak drift velocity and the threshold field.

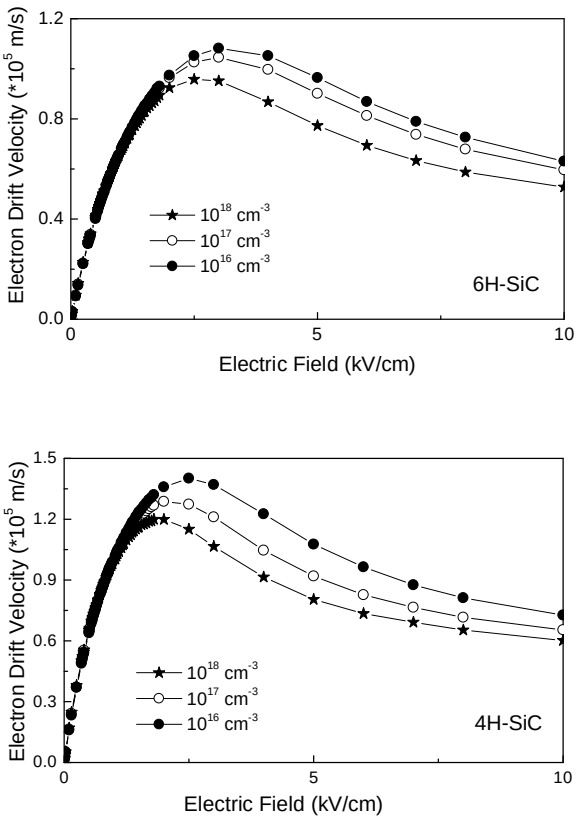

Figure 5: Calculated electron steady-state drift velocity in bulk 6H-SiC and 4H-SiC as a function of applied electric field for various donor concentration at room temperature.

CONCLUSIONS

Electron transport at different temperatures in bulk 6H-SiC and 4H-SiC have been simulated using an ensemble Monte Carlo simulation. Using valley models to describe the electronic band structure, calculated velocity-field characteristics show that the inter-valley transitions in high electric fields play an important role, in spite of a large separation between the central and upper valleys. The inter-valley transitions lead to a large negative differential conductance. Saturation drift velocities of about 0.75×10^5 ms^{-1} match recent measurements on low-doped bulk samples. We have also demonstrated that low temperature sensitivity of the electron transport properties of 6H-SiC and 4H-SiC are attractive for high-temperature and high-power electronic applications.

ACKNOWLEDGEMENTS

This work is supported by the Ferdowsi University of Mashhad through a contract with Vice President for Research and Technology.

REFERENCES

[1] A.Tsukazaki, A. Ohtomo, T. Onuma, M. Ohtani and M. Kawasaki, *Nat. Mater*., 4, (2005), 42.
[2] T. Makino, Y. Segawa, A. Ohtomo, *Appl. Phys. Lett*. 78, (2001), 1237.
[3] T. Makino, K. Tamura and C. H. Chia, *Phys. Rev.* B 65, (2002), 121201.
[4] E. Bellotti, B. K. Doshi and K. F. Brennan *J. Appl. Phys*. 85, (1999), 916.
[5] D. C. Look, D. C. Reynolds, J. R. Sizelove, and W. C. Harsch, *Solid State Commun.* 105, (1998), 399.
[6] Y. Chen, D. M. Bagnall, H. J. Koh, K. T. Park, Z. Q. Zhu and T. Yao, *J. Appl. Phys*. 84, (1998), 3912.
[7] C. Moglestue, Monte Carlo Simulation of Semiconductor Devices, (Chapman and Hall. 1993) p. 120.
[8] C. Jacoboni and P. Lugli, The Monte Carlo Method for semiconductor and Device Simulation, (Springer-Verlag. 1989) p.87.
[9] B. K. Ridley, Electrons and phonons in semiconductor multilayers, (Cambridge University Press. 1997) p. 121.
[10] D. Chattopadhyay and H. J. Queisser, *Review of Modern Physics*, 53, (1981), 67.
[11] K. Di. and K. Brennan, J. Appl. Phys. 69, (1991), 3097
[12] N. Mansour, K. Di. and K. Brennan, *J. Appl. Phys.* 70, (1991), 6854.
[13] H. Arabshahi, M. R. Benam and B. Salahi, *Modern Physics Letters* B. 21, (2007), 1715.
[14] H. Arabshahi, *Modern Physics Letters* B. 21, (2007), 199.
[15] K. Shimada, T. Sota and K. Suzuki, *J. Appl. Phys*., 84, (1998), 4951.
[16] R. P. Joshi, Appl. Phys. Lett., 64, (1994), 223.
[17] H. Arabshahi, *Modern Physics Letters* B. 21, (2007), 287.
[18] M V Fischetti, *Phys. Rev.* 44, 5527 (1991)
[19] B K Ridley, Electrons and phonons in semiconductor multilayers, Cambridge University
[20] C Erginsoy, *Phys. Rev.* 79, 1013 (1950).
[21] C Schwartz, *Phys. Rev*. 124, 1468 (1961)
[22] M V Fischetti, *Phys. Rev.* 44, 5527 (1991)
[23] H Morkoc, Nitride semiconductor and devices, Springer-velag (1999)
[24] Udayan, V Bhapkar and M S Shur, *J. Appl. Phys*. 82, 1649 (1997)